Conf-780811--9

MASTER

LA-UR - 78 - 1910

TITLE: RECENT DEVELOPMENTS IN LINEAR THETA-PINCH AND LASER-HEATED SOLENOID RESEARCH

AUTHOR(S): K.F. McKenna, R.R. Bartsch, R.J. Commisso, C.A.Ekdahl, K.B.Freese, R.F.Gribble, F.C.Jahoda, G.Miller, R.E.Siemon, J.U.Brackbill, J.P.Freidberg, S.P.Gary, H.R.Lewis, A.G.Sgro, L.Turner, D.Winske, A.L.Hoffman,* E.A.Crawford,* D.D.Lowenthal,* D.C.Quimby,* G.C.Vlases,** H.W.Hoida,** and Z.A.Pietrzyk**

SUBMITTED TO:

Seventh International Conference on Plasma Physics and Controlled Nuclear Fusion Research, 23-30 August 1978, Innsbruck, Austria. IAEA-CN-37-U-5

*Mathematical Sciences Northwest, Inc., Bellevue, Washington, USA

**University of Washington Seattle, Washington, USA

los Alamos
scientific laboratory
of the University of California
LOS ALAMOS, NEW MEXICO 87544

An Affirmative Action/Equal Opportunity Employer

No. 836
5, 2/80

UNITED STATES
ENERGY RESEARCH AND
DEVELOPMENT ADMINISTRATION
CONTRACT W-7405-ENG. 36

Seventh International Conference on Plasma Physics
and Controlled Nuclear Fusion Research

23-30 August 1978, Innsbruck, Austria

IAEA-CN-37-U-5

RECENT DEVELOPMENTS IN LINEAR THETA-PINCH AND LASER-HEATED SOLENOID RESEARCH*

K. F. McKenna, R. R. Bartsch, R. J. Commisso, C. A. Ekdahl,
K. B. Freese, R. F. Gribble, F. C. Jahoda, G. Miller, R. E. Siemon,
J. U. Brackbill, J. P. Freidberg, S. P. Gary, H. R. Lewis,
A. G. Sgro, L. Turner, and D. Winske
Los Alamos Scientific Laboratory, University of California,
Los Alamos, New Mexico 87545, USA

A. L. Hoffman, E. A. Crawford, D. D. Lowenthal, and D. C. Quimby
Mathematical Sciences Northwest, Inc.,
Bellevue, Washington, USA

G. C. Vlases, H. W. Hoida, and Z. A. Pietrzyk
University of Washington
Seattle, Washington, USA

ABSTRACT

Experimental and theoretical investigations of end-loss, end-stoppering, stability, and heating in linear theta pinches have been conducted. Efforts of groups at the Los Alamos Scientific Laboratory (LASL), Mathematical Sciences Northwest (MSNW), and the University of Washington (UW) are reported. At LASL, the experimental results from the high energy ($T_e + T_i = 3.3$ keV, $n_e = 1.5 \times 10^{16}$ cm^{-3}) 5-m Scylla IV-P theta pinch support the following; (1) Single mode m=1 "wobble" instability rotation frequencies of ~ 180 kHz are associated with axial wavelengths of 400-800 cm. (2) Ion thermal conduction is an unimportant loss mechanism. (3) Evidence of rarefaction-like waves is seen. (4) The normalized end-loss

time is independent of the plasma beta and collisionality regime. (5) Plasma flow from the ends remains collimated and convects magnetic fields. (6) LiD end plugs produce a three-fold increase in energy containment time over the open-ended configuration. Theoretical work at LASL has demonstrated the following; (1) An explanation of the m=1 "wobble" instability has been formulated. (2) A correct description of end-loss must include the magnetic curvature term in the axial momentum equation. Mirrors increase the lifetime of a collisional plasma less than guiding center theory predicts. (3) Magnetic field gradient drift can reduce the growth rate of the universal drift instability. (4) Collisionless magnetoacoustic heating can be an effective heating mechanism in theta pinches. At MSNW-UW, CO_2 laser heating of low energy ($T_e \simeq T_i \simeq 2$ eV, $n_e \simeq 2 \times 10^{17}$ cm^{-3}) plasmas is accomplished over a one-meter column length. Maintenance of a on-axis density minimum is demonstrated.

*Work performed under the auspices of the U. S. Department of Energy.

INTRODUCTION

High energy thermonuclear plasmas can be generated in linear theta pinches. Areas of current interest in the fusion application of these devices include end-loss, stability, and heating. End losses, which present a fundamental limitation on the plasma energy containment time, result from particle loss through the theta-pinch open ends and axial thermal conduction losses along the magnetic field lines. To obtain relevant fusion reactor designs, the detailed mechanisms involved in these end-loss processes must be identified and effective end-stoppering techniques developed. In addition, an understanding of the plasma stability characteristics is required; the m=1 "wobble" is the only observed MHD instability of significance in high energy theta-pinches. The development of alternative plasma heating techniques would also enhance the theta-pinch reactor concept and reduce the technological demands presented by implosion heating.

In this paper experimental and theoretical studies of end-loss, end-stoppering, stability, and heating in linear theta pinches are presented. Efforts of groups at the Los Alamos Scientific Laboratory (LASL), Mathematical Sciences Northwest (MSNW), and the University of Washington (UW) are reported. Experiments on the LASL high energy Scylla IV-P theta pinch have been directed towards the investigation of particle and thermal losses, the plasma flow and magnetic field interaction processes near the coil ends, end-loss suppression using solid material end plugs, and the plasma stability characteristics. Theoretical efforts at LASL have dealt with the driving mechanisms of the observed m=1 "wobble" instability, numerical studies of particle end-loss, instability effects on radial diffusion, and magnetoacoustic heating methods. The interaction of CO_2 laser radiation with theta-pinch like plasma columns is being studied at MSNW and UW. In these experiments the channeling of the laser light along the axis of a partially ionized plasma column, and the resultant heating is investigated.

1. ...L SCYLLA IV-P THETA-PINCH EXPERIMENTS WITHOUT END PLUGS

1.1. Theta-Pinch Experimental Arrangement. Scylla IV-P has a maximum energy storage of 2 MJ at 60 kV primary bank voltage. Six-hundred 1.8-μF capacitors feed the 500-cm long, 11.2-cm dia. single-turn compression coil. Primary bank operation at 45 kV generates a vacuum E_0 of 0.6 kV/cm at the inside wall of the 8.8 cm i.d. quartz discharge tube and a peak compression field, B_z, of 4.8 T is obtained 3.1 μs after discharge initiation. A crowbar system extends the magnetic field in time with an L/R decay of 110 μs. The experimental results discussed below are obtained at 45 kV primary bank voltage and with a theta-pinch fill pressure of 10 mTorr D_2. To provide access for optical and internal plasma diagnostics in the theta-pinch end regions, each end of the discharge tube is terminated, 4.5 cm beyond the coil ends, within a quartz expansion chamber. The chambers are 20-cm in dia., 45-cm long, and end-supported by 20-cm dia. metal vacuum tees.

1.2. Plasma Parameters. The plasma column total particle inventory, N_e, and axially averaged peak density, n_a, are determined from holographic ruby laser end-on interferograms. Near the time of peak magnetic field when the plasma column is highly symmetric and instability free, the plasma radius, a, is obtained from the interferometrically measured radial density profiles; a correction for refractive bending of the interferometer laser light is applied. The onset of a finite wavelength m=1 instability at $t \simeq 5$ μs distorts the radial density profiles recorded on the interferograms. The plasma radius is then determined from the relation $a = (N_e/\pi n_a L)^{1/2}$, where L is the coil length. It should be noted that the low density plasma "halo" observed to surround the central plasma column for times $t \gtrsim 15$ μs is not included in the interferogram analysis. A diamagnetic loop and probe arrangement at the coil midplane is used to measure the magnetic flux, $\Delta\phi$, excluded by the plasma. The excluded flux measurement is combined with the plasma radius data to obtain the peak plasma beta, β_a. The total plasma temperature is estimated from pressure balance, $T_e + T_i = \beta_a B_z^2/n_a k 8\pi$. The electron temperature, T_e, also measured at the coil midplane, is determined from 90° Thomson scattering. The peak magnetic field plasma parameters are: $n_a \simeq 1.5 \times 10^{16}$ cm^{-3}, $T_e + T_i \simeq 3.3$ keV, $T_e \simeq 570$ eV, $\beta_a \simeq 0.9$ and $a \simeq 1.0$ cm. At t = 6.0 μs, after the magnetic field has passed through its maximum oscillation and the crowbar has become effective, the plasma parameters are: $n_a \simeq 0.9 \times 10^{16}$, $T_e + T_i \simeq 2.3$ keV, $T_e \simeq 440$ eV, $\beta_a \simeq 0.6$ and $a \simeq 1.2$ cm.

1.3. Plasma Stability. The plasma stability characteristics are determined from side-viewing stereo streak photographs and an axial array of 18 (9 vertical and 9 horizontal viewing) optical plasma-position detectors. Figure 1 presents a typical stereo streak photograph taken near the coil midplane. The upper streak shows the plasma viewed from the top of the coil, and the lower streak shows the plasma viewed from the coil front. The slight curvature evident at early times ($t < 5$ μs) results from the effect of the theta-pinch magnetic field on the camera image converter tube. The MHD stable plasma column is disrupted by the onset of the m=1 "wobble" instability at $t \simeq 5$ μs, which is about the time required for an Alfvén wave to propagate from the theta-pinch ends to the midplane. The following characteristics of the "wobble" instability have been identified: (1) The column rotates in the direction expected for ion rotation. (2) When the column displays a single mode, it rotates in a plane with a node near the coil midplane. (3) Single mode rotation frequencies of 180 ± 80 kHz are associated with wavelengths of 400 to 800 cm; however, frequencies of about

twice this value have been observed in conjunction with wavelengths of 200 to 400 cm during at least part of the discharge in localized regions of the pinch. (4) The peak amplitude of the motion is about 2 cm.

Despite a substantial number of theoretical investigations of plasma rotation in theta pinches, only recently has an adequate explanation for the m=1 "wobble" instability been provided [1]. The plasma stability is determined by solving the eigenvalue problem for the rotating plasma as described by the finite Larmor radius fluid equations including the effects of finite β and $k^2 \neq 0$, where k is the disturbance axial wavenumber. The results of these calculations indicate that the stability threshold, measured in terms of rotation, for the experimentally-observed m=1, n=0 mode is the lowest of any mode (including m=2, n=0 and m=1, n=1), and in this sense it is the worst mode (m is the azimuthal mode number and n the number of radial nodes). Contrary to early intuition, the fastest m=1, n=0 growth rate occurs for $k^2 > 0$, while $k^2 = 0$ is neutrally stable. When both the m=1, n=0 and m=2, n=0 modes are unstable, the growth rate for the latter is greater than the m=1, n=0 growth rate by a factor of about 5. Good agreement with the Scylla IV-P experiment is obtained by assuming that plasma conditions are near the completely end-shorted state, and that the column has a small positive charge (as arises from ambipolar potentials). In particular, the plasma parameters appear to be in the regime where only m=1, n=0 is unstable, and m=2, n=0 is below threshold. For complete shorting and no column potential, the theory predicts neutral stability in contradiction to the experimental observations noted above.

1.4. Energy and Particle Containment. The time histories of the total plasma temperature and electron temperature are shown in Fig. 2. The total temperature has been experimentally determined both from pressure balance, and from estimates of the ion temperature obtained from the neutron emission rate (measured with plastic scintillation detectors) combined with the electron temperature from Thomson scattering. The solid lines indicate the results of a recently-developed time dependent, zero-dimensional MHD particle and heat-flow code [2], which is used here to model the plasma conditions at the coil midplane. The low values of measured T_e, relative to $T_e + T_i$, result from preferential ion heating during the implosion phase and electron heat conduction to the cold material walls at the theta-pinch ends. For $t > 10$ μs, the zero-temperature boundary condition MHD code, which utilizes classical electron thermal conduction, predicts T_e in agreement with experiment. Delaying the onset of electron thermal conduction for 3-6 μs in the code results in electron temperature predictions which are in good agreement with all the experimental data points. This suggests that a finite time is required for the plasma to flow from the theta-pinch ends, contact a cold material wall, and establish a zero-temperature boundary condition.[1] The characteristic electron thermal conduction time, approximated as $\tau_c^e \simeq (3/2)\, n_e k (L/2)^2 / K_\parallel^e$ where $K_\parallel^e$ is the parallel electron thermal conductivity, is about 1.5 μs at peak field.

[1] As pointed out by Dr. H. R. Griem, the question of energy deposition by electron thermal conduction to the relatively cold plasma flow in the expansion chambers remains unresolved.

The time history of $T_e + T_i$ predicted by the MHD code generally overestimates the measured total temperature decay rate. However, the code does indicate that the ion temperatures are several times greater than the electron temperatures, as observed experimentally, and is obtained by eliminating ion thermal conduction losses in the simulation. Experimentally, the ions are collisionless and thus classical ion thermal conduction, which is a diffusive process resulting from ion-ion collisional interactions, cannot be supported. The ion-ion mean free path, λ_{ii}, is ~ 700 cm at peak field and approaches L only at late times, $t > 30$ μs; $\lambda_{ee} \simeq 30$ cm at peak magnetic field. Accordingly the ions are collisionless throughout the observed plasma lifetime while the electron population remains collision dominated. The ions lose energy via axial convection and by energy transfer to the lower energy electrons. Ion energy transfer to the collisional electron population accounts for the observed slow decay of T_e compared to τ_c^e. Based on the peak field parameters, the e-folding time constant for ion-electron energy transfer is about 40 μs.

The total plasma energy per unit length, E_ℓ, is obtained from measurements of $\Delta\phi$ and B_z. Using the pressure balance condition and approximating the peak beta as $\beta_a = 2\,\Delta\phi/B_z \pi a^2$, E_ℓ can be expressed as $E_\ell = B_z \Delta\phi/4\pi$. Figure 3 presents the time history of E_ℓ measured at the theta-pinch midplane. The solid line gives the results of the MHD code. For $t < 5$ μs, E_ℓ is dominated by the rapid rise and fall of B_z. The quiescent period between 5 and 7 μs in which E_ℓ remains constant is terminated by the onset, at $t \simeq 7$ μs, of an abrupt decay. This observation cannot be explained by the gradual decay in B_z but rather results from the onset of convective energy losses at the coil midplane. In collisional plasmas, the onset of convective losses is initiated by the arrival of rarefaction waves from the plasma column ends at $t = L/2V$, where V is the wave speed. The results of the collisional Scylla I-C experiment suggest that the rarefaction waves propagate inward at the cusp speed U [3]. For the Scylla IV-P experiment $L/2U \simeq 7$ μs which corresponds to the observed E_ℓ decay onset time; axial flow is initiated in the code at this time. A kinetic treatment [4] of the end-loss processes in collisionless plasmas predicts transient phenomena similar to collisional rarefaction waves. The estimated onset time of convective losses from the kinetic approach is in qualitative agreement with experiment [5]. Thus, although the detailed processes involved in the communication of the theta-pinch ends with plasma at the midplane are different in collisional and collisionless plasmas, the observed large-scale phenomena are similar, i.e., what would appear to be inward propagating "waves" can be identified in both collisionality regimes.

The time evolution of the electron inventory, N_e, of the central plasma column, obtained from the end-on interferograms neglecting the "halo" plasma, is presented in Fig. 4. The basic phenomenology of the inventory time history is identical to that observed in previous high-energy theta-pinch experiments. Specifically, N_e remains constant for an initial period of about 6 to 8 μs duration before an exponential decay is observed. The cause of this initial plateau has been identified in the present experiment and will be discussed below. A least squares fit to the data of Fig. 4, for $t \gtrsim 6$ μs, yields an e-folding end-loss time τ of 12.5 ± 0.5 μs.

1.5. Plasma Flow from the Theta-Pinch Ends. The characteristics of the plasma flow into the end expansion chambers are studied photographically, spectroscopically, with magnetic flux loops, and internally with magnetic field probes and a pressure probe sensitive to

local particle momentum flux [5]. The plasma flow out of the theta-pinch ends is preceded by an axially outward propagating shock wave initiated during the implosion phase and identified photographically and from local pressure measurements. The impact pressure of the out-flow plasma following the shock wave is measured with a 2 mm dia. acoustic delay line piezoelectric pressure sensor inserted axially into an end expansion chamber. Local pressure measurements are made at various axial positions between the coil end and 26 cm downstream from the end, and extend radially over the diameter of the expansion chamber. From the pressure measurements [5,6] a highly collimated (little radial expansion) axial plasma flow is observed for the entire duration of the experimental observation time (~ 40 μs). The axially-flowing plasma is believed to expand to the walls as it enters the metal vacuum tees located ~ 50 cm from the coil ends. The collimation of the end-flow plasma results in the initial period of constant electron inventory observed interferometrically. Since the end-on interferometer responds to all the electrons within the laser beam path, and since the plasma front following the initial shock wave does not expand out of the interferometer field of view for several microseconds no decrease in N_e will be detected during this time.

From local magnetic field probe measurements, exclusion of the magnetic field from the expansion chamber is observed until after passage of the shock wave. Near the expansion chamber axis, the magnitude of the magnetic field within the plasma following behind the shock wave exceeds the vacuum field value. These results not only indicate that the magnetic field structure external to the theta-pinch coil is distorted in the presence of plasma but also that magnetic field is "frozen" into the plasma and convected axially with the flow.

1.6. Particle End-Loss Time. In the determination of the end-loss time τ, the data within the period of artificially constant N_e ($t < 6$ μs) was not included in the analysis. To obtain a consistent comparison, the electron inventory data from previous high-energy theta-pinch experiments have been re-analyzed neglecting the period of constant N_e. For comparison with theory the measured particle end-loss time is expressed as $\tau = (L/2)[m_i/2k(T_e + T_i)]^{1/2}\ \eta$, where η is a normalizing parameter representing the ratio of measured end-loss time to thermal-transit time. In Fig. 5, η is plotted against β_a. The solid lines identify existing theories, reviewed in Ref. [7] and the X's mark the results of a recent numerical treatment [8] discussed in section 3.1.. The data points (based on peak field plasma conditions) are from the collisionless Scylla IV-P, Scylla IV-3 [9] and linear Scyllac [10] experiments and the collision-dominated Scylla I-C experiment [3]. Examination of Fig. 5 indicates the following: (1) for all experiments the measured particle end-loss times are between 2.2 and 2.8 thermal transit times, (2) the experimental values of η do not display an identifiable dependance on β_a, and (3) the experimental values of η are independent of the plasma collisionality regime.

2. LASL SCYLLA IV-P THETA-PINCH EXPERIMENTS WITH SOLID END PLUGS

End-stoppering experiments using solid silicon dioxide (quartz), boron nitride (BN), and lithium deuteride (LiD) end plugs have been performed on Scylla IV-P. The plugs are cylindrically shaped, 5 cm in diameter and 3.8 cm thick. The front face of each plug is inserted ~ 5 cm inside the ends of the theta-pinch coil. Initial experiments [11] using the quartz plugs demonstrated the following: (1) the stability of the plasma column is

improved compared to the open-ended case, the m=1 instability being rapidly damped, (2) plasma does not flow past the plugs and out of the theta-pinch ends, (3) the total plasma neutron yield measured with the plugs inserted is about equal to that measured without the plugs. Ablation of the quartz plug surface amounted to less than 1 μm of plug material ablated per discharge, with about 0.1 % of the plasma energy invested in the ablation process. Only a slight increase (~ 20%) in energy-confinement was measured with the quartz plugs. Particle and energy flow to the end-plug region and energy losses by atomic proces s (primarily radiation) in this region dominated the energy confineme e theta-pinch midplane. In an attempt to reduce the energy loss by processes, more recent experiments have been conducted using the (Z = atomic number) BN and LiD plugs. Results (1)-(3) noted above a so observed in the BN and LiD end-plug experiments.

2.1. Density Measurements in the Plasma-Plug Interaction Region. Side-viewing ruby laser interferometry is used to observe the ablated plasma near the end-plug surface. Figure 6 presents radial density profiles determined from Abel inversion of the interferometer fringe shift profiles recorded at early times during the discharge for the BN and LiD end plugs. For the BN plugs (Fig. 6a) the density profile close to the plug face (z=0.1 cm) is nearly Gaussian with an e-folding radius about equal to that of the plasma column radius and with peak densities resulting from ablation and subsequent ionization in excess of 5×10^{18} cm^{-3}. At axial positions $z > 0.1$ cm the ablated BN plug material is concentrated at the outer edge of the column where the axial pressure is less than on the column axis, resulting in annular density profiles. The axial electron line density is determined from area integration over the BN plug radial density profiles. Analysis of the line density profiles shows that the ablation layer formation time is 1-1.5 μs and that the layer attains a thickness of about 1 cm at $t \simeq 5$ μs. After this time the line density slowly decreases, indicating an attenuation in the plug material ablation rate. With the BN end plugs the time history of E_ℓ, measured at the coil midplane, is approximately the same as that measured with the quartz plugs.

LiD is the lowest-Z solid end-plug material available at room temperature. The line radiation from this material should be burned through at an electron temperature of 100 eV. Side-on interferograms obtained with the LiD plugs indicate a higher density of ablated plug material than observed for the BN end-plugs. A sufficient quantity of plug material is ablated and ionized in the first two microseconds of the discharge such that the interferogram fringes within a centimeter of the plug face are completely obscured. Typical radial density profiles obtained with the LiD end plugs are shown in Fig. 6b. As with the BN plugs a high electron density is observed at the outer edge of the plasma column. However, with the LiD plugs a high ablated plug material electron density is also measured along the plasma column axis. From line density analysis, the ablation layer formation time is about 1-2 μs. The layer attains a thickness of about 3 cm at $t \simeq 5$ μs. The ablation process is attenuated for $t > 5$ μs.

2.2. Energy Line-Density Measurements with LiD End Plugs. With the LiD plugs, E_ℓ measurements at the theta-pinch midplane show a significant increase in energy confinement time over that obtained in the open-ended geometry and with higher-Z end plugs. The time history of E_ℓ with and without the LiD plugs is presented in Fig. 7. With the LiD plugs the energy containment time, τ_E, is increased over a factor of three (from 9 to 29 μs)

above that measured with open ends. This result is in agreement with the MHD code calculations shown in Fig. 3, in which the axial plasma flow is stopped and the decay of the midplane plasma energy is dominated by electron thermal conduction to non-radiating ablated plug material and the decay of the confining magnetic field. The calculated [12] line and continuum radiation losses from the LiD plugs are significantly less than that from the higher-Z plugs. In addition, a much higher density of ablated material is experimentally observed to propagate into the plasma column with LiD plugs than with the BN plugs. These results indicate that radiation losses with the LiD plugs are small enough to permit the formation of an ablation zone of sufficient pressure to impede the axial flow and associated energy losses of the deuterium plasma.

3. LASL LINEAR THETA-PINCH THEORETICAL RESEARCH

3.1. Endloss Studies. The computed η values shown in Fig. 5 by the X's are the result of a study of end-loss in which the time-dependent equations for magnetohydrodynamic flow in two dimensions are solved numerically [8]. Other qualitative results of this study are: (1) The total mass in a theta pinch decays exponentially in time due to end-loss with an end-loss time which is proportional to length. (2) The end-loss time is insensitive to the boundary conditions at the outflow ends. That is, the end-loss time with free expansion at the end, as in the case of a long guide field, is virtually identical to the end-loss time with zero pressure, as in the case of a high-Z end plug. (3) The end-loss time, normalized to the thermal transit time, η, is significantly different from other theories (c.f. Fig. 5), especially in its lack of dependence on the plasma beta [7]. The end-loss time agrees relatively well with experimental data.

A study of the results of the numerical calculations indicates the magnetic field curvature term contributes significantly to the axial momentum equation, and may account for the difference between the results of two-dimensional and one-dimensional solutions of the time dependent equations [13]. The axial momentum equation is written as follows,

$$\rho\left(\frac{\partial w}{\partial t} + u\,\frac{\partial w}{\partial r} + w\,\frac{\partial w}{\partial z}\right) + \frac{\partial p}{\partial z} = B_r\,\frac{\partial B_z}{\partial r} - \frac{\partial}{\partial z}\left(\frac{B_r^2}{2}\right)$$

$$+2 \qquad 0 \qquad 4 \qquad -9 \qquad -3 \qquad 0 \quad ,$$

where ρ and p are the plasma density and pressure, u, B_r, w and B_z, the components of velocity and magnetic field in r and z respectively. Below each term is its typical relative value in the numerical solutions. Note that $B_r \partial B_z/\partial r$ is comparable to $\partial p/\partial z$, and therefore will have a significant effect on the axial flow. The absence of this term, among others, in the one dimensional approximation probably accounts for the difference in the computed values of η between the one- and two-dimensional solutions. (The simplest description of end-loss may result from the long, thin approximation, $a/L \ll 1$, where a is the plasma radius and L the length of the theta pinch [14]. In this approximation, only the last term in the above equation is $O((a/L)^2)$ and may be deleted. However, no comparable solutions of the ordered equations are available.)

The results of a study of the effect of single mirrors on plasma confinement are shown in Fig. 8. There, the variation of n with mirror ratio, M, is shown for $0.25 \leq M \leq 4$, and compared with measurements made on linear Scyllac [10]. In agreement with that experiment, the mirrors reduce end-loss, but much less effectively than guiding center theory predicts.

3.2. Magnetic Gradient Effects on the Universal Instability. The density gradient driven universal instability is expected to govern radial diffusion in theta-pinch plasmas on fusion time and distance scales since, unlike other cross-field instabilities, it is unstable for arbitrarily small density gradients. However, finite plasma beta (either due to the inclusion of magnetic gradient or electromagnetic effects) tends to reduce the growth rate of the universal instability and can even stabilize it [15]. Here the linear Vlasov theory of the universal instability in a unidirectional magnetic field ($\mathbf{B} = \hat{z}B$) is considered in the slab model with the local approximation in the electrostatic limit but including the full resonant effects of a magnetic field gradient drift. Inclusion of the ∇B drift requires expression of the linear dispersion relation in terms of an integral over $v_\perp$, the perpendicular drift speed. Solutions to the dispersion relation computed without approximation demonstrate that the effect of a magnetic field gradient (expressed here in terms of the local ion beta, $\beta_i = 8\pi nkT_i/B^2$) is to reduce the maximum growth rate γ_m of the universal instability. Numerical analysis demonstrates that the ion ∇B effects are more important than the corresponding electron contributions, but that both act to reduce the growth rate. The increased damping is due to velocity space broadening of the electron Landau resonance driving term and a similar extension of the ion Landau damping term into the resonant ion region. The velocity broadening of the electron resonance is small compared to the width of the electron distribution, and these computations have demonstrated that expansion of the electron susceptibility to first order in the reciprocal magnetic gradient scale length (ϵ_B) yields results equivalent to those from the full integral. However, a relatively small value of β_i brings the ∇B resonance well into the ion distribution, and various approximations to the ion susceptibility fail as β_i increases. One approximation, an expansion of the ion susceptibility to first order in ϵ_B, yields a maximum growth rate that agrees with the exact result to within a few percent for only rather low values of β_i, $\beta_i < 0.02$, and is roughly 60% larger at modest β_i, $\beta_i = 0.2$, for typical parameters ($T_i = T_e$, $m_i = 3674\, m_e$, ratio of electron-ion relative drift speed to ion thermal speed = 0.05). A second approximation, which involves replacing the $v_\perp^2$ factor in the Fried-Conte function with $2\, T_i/m_i$, is somewhat better. The maximum growth rate computed with this approximation agrees with the exact result to within 2% for $\beta_i < 0.08$ and is only 20% larger at $\beta_i = 0.2$.

3.3. Magnetoacoustic Heating. Magnetoacoustic heating is an attractive method for preferentially heating plasma ions when an appropriate dissipative mechanism exists at a convenient magnetoacoustic resonant frequency. The observations of collisionless damping of magnetoacoustic waves in a high-beta plasma [16] are experimental evidence for the existence of a dissipative mechanism in a collisionless plasma. For a linear theta pinch, magnetoacoustic heating would not impose a limitation on end-stoppering schemes. With a judicious choice of parameters, magnetoacoustic heating may allow the use of lower values of induced RF electric fields than are required when implosion heating is the sole method of heating.

We have studied theoretically the physics relevant to magnetoacoustic heating of a screw pinch (equivalent to a theta pinch when $B_\theta = 0$) in a collisionless plasma regime by two approaches and we are applying the results to cases of experimental interest. Heating times and associated induced RF electric fields have been computed. Both approaches are based on the Vlasov-fluid model [17] in which collisionless ions and massless, fluid electrons are treated under the assumptions of quasi charge neutrality and negligible displacement current. The two approaches differ with respect to their ordering of small parameters and with respect to their treatment of the boundary between the plasma and a surrounding vacuum. In the first treatment, [18] the techniques of earlier analyses [19] have been combined with an ordering scheme adapted to the study of magnetoacoustic waves. The basic smallness parameter is the ratio (ion gyroradius)/(plasma radius); in terms of that parameter, the quantities local plasma beta, (plasma radius)/(any scale length of the wave), and (phase velocity along the magnetic field)/(ion thermal velocity) are assumed to be of order unity. This ordering scheme applied to the Vlasov-fluid model provides a physical description of the plasma which contains kinetic effects along the magnetic field lines but retains only fluid-like effects transverse to the field lines; finite-ion-gyroradius effects do not contribute in leading order. A basic result of applying this description to a pinch configuration is the identification of ion Landau damping as a viable dissipative mechanism for converting magnetoacoustic wave energy into ion thermal energy [18]. The Landau damping causes a phase shift in the response of the plasma relative to the phase of an imposed oscillation of the confining magnetic field; this shift is responsible for the dissipation. At a magnetoacoustic resonance the amplitude of the plasma response and the associated rate of dissipation peak. The total rate of energy dissipation is obtained by calculating the Poynting vector external to the plasma column. That the energy dissipated is converted completely into ion thermal energy is proved by use of a thermal transport equation derived from the ion Vlasov equation. In order to obtain the shortest doubling time, τ_d, for the plasma energy with the least induced RF electric field, E, it appears desirable to operate at a ratio of (phase velocity along the magnetic field)/(ion thermal velocity) roughly equal to 0.7. For theta pinch parameters, we have obtained τ_d's on the order of 10^{-4} s with fields E on the order of 80V/cm.

In the second approach, the effect of finite ion gyroradius on magnetoacoustic heating of a sharp-boundary screw pinch is being studied. In order to take proper account of the sharp boundary, the starting equations are those derived previously for applying the Vlasov-fluid model to a sharp-boundary screw pinch [20]. Within the pinch the collisionless Boltzmann equation for the Vlasov-fluid model has been solved analytically for small values compared to unity of kr_L and ω/ω_{ci}, where k is the largest relevant wavenumber, r_L is the ion gyroradius, ω is the frequency, and ω_{ci} is the ion cyclotron frequency. Finite-ion-gyroradius effects were kept to zeroth and first order and the solution is valid up to the sharp boundary. Because this approach uses a more general ordering, it also should be possible to determine whether dissipative mechanisms other than Landau damping are operative for magnetoacoustic heating in a collisionless plasma. A differential equation for $\underset{\sim}{\xi}$ ($\underset{\sim}{A}^{(1)} = \underset{\sim}{\xi} \times \underset{\sim}{B}^{(0)}$ where $\underset{\sim}{A}^{(1)}$ = perturbation vector potential and $\underset{\sim}{B}^{(0)}$ = equilibrium magnetic field) containing finite gyroradius effects was derived by substituting the solution of the collisionless Boltzmann equation into the transverse force-balance equation (the component perpendicular to $\underset{\sim}{B}$ of the Maxwell $\underset{\sim}{\nabla} \times \underset{\sim}{B}$ equation). An analytical solution of the equation for $\underset{\sim}{\xi}$ was used to calculate the heating of the

pinch in the presence of an oscillatory driving electric field on a cylindrical surface in the vacuum region surrounding the pinch [21]. Numerical studies have been made to examine the primary m=0 magnetoacoustic resonance in sharp-boundary pinches whose equilibrium parameters were chosen to model the staged theta pinch experiment at LASL [22]. The dependence of the heating rate upon r_L/r_o and kr_o was investigated, where r_o is the pinch radius. The numerical results, which are quite similar for both experiments, can be summarized as follows: 1) For large axial wavelengths ($kr_o < 0.01$), the resonance is extremely narrow and is little affected by changes in r_L/r_o. Because of the narrowness of the resonance, absorption of such long wavelength waves is uninteresting as a practical heating mechanism. 2) For axial wavelengths such that $kr_o \simeq 2$, the resonance is quite different. For example, with $r_L/r_o = 0.01$, the full width at half maximum is in the range of a few to several percent, and maximum values of Q (the heating rate normalized to the plasma kinetic energy) in the range of $0.0005\ \omega_{ci}$ to $0.02\ \omega_{ci}$ have been computed for a driving electric field of 50 V/cm. The rate of collisionless absorption for these short axial wavelengths can be very large and may provide a useful heating mechanism for fusion experiments. The plasma response and the heating rate $\underset{\sim}{j}\cdot\underset{\sim}{E}$ exhibit radial structure whose scale length is of the order of r_L.

4. MSNW-UW CO_2 LASER HEATED SOLENOID RESEARCH

The laser heated solenoid fusion concept was formulated to take advantage of the fortuitous match between the absorption length for CO_2 laser radiation at 10.6 μm of reactor grade plasmas and the length needed to achieve net energy output from open-ended linear reactors. The principal requirement of this approach is the necessity of channeling the laser radiation along the centerline of a solenoidal magnet over long column lengths through the formation and maintenance of an on-axis electron density minimum in the plasma. This minimum can be created either by laser breakdown of a neutral gas in a steady magnetic field or by a combination of laser heating and theta pinch implosion in a rising magnetic field. The latter method, by which the plasma is removed from the wall, is the subject of the present experiments. In this case, the density minimum must be maintained against diffusive erosion from the vacuum boundary.

Beam propagation and heating has been investigated in two separate experiments, one at MSNW employing several kJ's of CO_2 laser radiation in a 2 μs pulse to heat plasma columns contained in a 1-meter long, 3.8 cm bore solenoid producing a magnetic field rising to 6 T in a 4.7 μs. Experiments at the UW utilize a 1 kJ laser and a 22-cm long, 3.3 cm bore solenoid producing a magnetic field rising to 14 T in 4.2 μs.

4.1. One-Meter Experiment (MSNW). The MSNW experiment is described in detail in Ref. [23]. A 35-cm diameter annular laser beam is focused to a 2 mm spot size by a 5-meter focal length mirror. Diamagnetic loops measure the excluded flux at either end and in the center of the solenoid. Cross-tube time dependent interferometry, radial streak photography, and time dependent spectroscopy are performed through slots at the magnet center. The entire vacuum chamber is statically filled with hydrogen or deuterium at pressures between 0.25 to 2.0 mTorr. The heating results at low and high pressures are remarkably different, reflecting the ability to maintain the on-axis density minimum necessary for beam trapping.

The gas in the magnet is preionized by a fast 12 kA Z-discharge lasting about 1.5 μs, and the main field capacitor bank is switched 2.5 μs later. Laser heating is initiated during the 300 ns implosion phase. The basic theta pinch produces a plasma compressed by a factor of 2 (at higher pressures) to 3 (at lower pressures) in diameter with a measured temperature of at most 2 eV. At the lower pressures ($p_0 \leq 1$ mTorr) laser heating raises the plasma to line energies of about 3 J/cm and peak temperatures of about 40 eV. This heating is nearly uniform along the column length, but decreases rapidly in effectiveness after about 1 μs into the laser pulse. Interferometric measurements indicate a loss of the required density minimum at this time, and lack of continued heating can be attributed to unfavorable beam refraction.

By contrast, laser heating is continuous throughout the 2 μs laser pulse for the higher fill pressures. There is a slight propagation delay in heating from one end of the column to the other, but the column is still heated nearly uniformly. Figure 9 shows a typical radial streak of the heated plasma at 1.0 mTorr D_2 fill pressure. The hydrodynamic bouncing is typical for high β. The diamagnetic signal in the center is compared in Fig. 10a with a one-dimensional, quasi-steady pressure balance model. This model cannot reproduce the hydrodynamic bouncing, but the agreement with the average measured diamagnetism is excellent, even though the calculated absorption length decreases to less than 1 m by the end of the 2 μs laser pulse. In contrast with the lower pressure results, the diamagnetic signal increases throughout the laser pulse, indicating very efficient beam trapping. The plasma energy inferred from the diamagnetic loop measurements increases after the laser pulse to a peak value of 8.5 J/cm.

Figure 10b shows the calculated plasma profiles as a function of time for this experiment. They show a density well persisting throughout the 2 μs laser pulse. Experiments carried out on a shorter solenoid in the UW experiment, where axial interferometry is possible, confirm this density minimum for high fill pressures. The appearance of the 3434 A^{O} C_{VI} line in spectrographic measurements confirms the peak calculated temperatures. Due to the high density, the electron and ion temperatures are nearly equal and the decay in peak temperature after the laser pulse is due to thermal conduction and radial equilibration. While the laser pulse is on, a strong thermoelectric effect produces a $\beta = 1$ condition in the center of the plasma, which is reduced due to diffusion to $\beta = 0.65$ at 4 μs. These experiments clearly indicate efficient beam trapping, maintenance of a density minimum, heating and subsequent adiabatic compression of the plasma. Based on this success, the magnet length is being extended to 3-m, the peak field to 15 T with a 8 μs rise time, and the laser energy increased to about 8 kJ in a 3-4 μs pulse length.

4.2. 22-cm Experiment (UW). Emphasis has been placed on axial interferometry in the UW experiments in order to accurately measure the radial electron density profile. Diamagnetic loops have been located at 5.5 cm and 16.5 cm in order to correlate the plasma line energy with the laser heated profiles. The evolution of density profiles produced by the theta pinch alone, for a fill pressure p_0 of 1.8 mTorr, is shown by the solid curves on Fig. 11. The plasma is only partially ionized, and an on-axis density minimum can be seen to be present during the 300 ns implosion, and after 500 ns. Strong laser heating was measured by both diamagnetic loops when laser heating was initiated before 300 ns or after 500 ns. Figure 12a shows a typical interferogram for the late time laser heating, and Fig. 12b shows

the plasma line energies inferred from the diamagnetic loop signals. Heated plasma electron density profiles are also shown by a dashed line on Fig. 11 for comparison with the unheated profiles. The electron density minimum is deepened, the total line density increases due to laser induced ionization, and the column expands significantly due to the increased energy content. Correlation of diamagnetic and interferometric data 1 μs into the laser pulse yields a centerline temperature, assuming a Gaussian temperature profile, of 60 eV, $\beta \simeq 1$, with $n_e = 3 \times 10^{17}$.

Details of these experiments are reported elsewhere [24]. Some further conclusions are; (1) timing of the laser pulse relative to the main field rise for efficient column heating is quite sensitive in small bore plasma tubes but should be less so in reactor size tubes, (2) peak temperatures in the UW experiments are governed by free streaming end losses, (3) laser energy addition reduces the tendency of the column to form flutes, (4) alignment of the laser beam is more critical at higher f numbers, (5) there is preliminary evidence that material end plugs substantially increase the plasma lifetime in accordance with predictions, and (6) wall light-up occurs on some shots and is believed to be due to refraction of the outer portions of the beam to the tube wall.

REFERENCES

[1] FREIDBERG, J. P. and PEARLSTEIN, L. D., Phys. Fluids 20 7 (1978) 1207.

[2] STOVER, E. K., ELEVANS, E. H., and YORK, T. M., Phys. Fluids (to be published).

[3] McKENNA, K. F. and YORK, T. M., Phys. Fluids 20 9 (1977) 1556.

[4] DRIECER, H., presented at the Third International Symposium on Plasma Heating on Toroidal Devices, Varenna, Italy (1976). Also available as Los Alamos Scientific Laboratory report LA-UR-76-2010 (1976).

[5] McKENNA, K. F., BARTSCH, R. R., COMMISSO, R. J., EKDAHL, C. A., JONES, I. R., and SIEMON, R. E. (to be published). Also available as Los Alamos Scientific Laboratory report LA-UR-78-1909 (1978).

[6] McKENNA, K. F., COMMISSO, R. J., EKDAHL, C. A., FREESE, K. B., KRISTAL, R., QUINN, W. E., and SIEMON, R. E., Eighth European Conference on Controlled Fusion and Plasma Physics, Prague, Czechoslovakia (1977), Vol. I, p. 85.

[7] FREIDBERG, J. P. and WEITZNER, H., Nucl. Fusion 15 2 (1975) 217.

[8] BRACKBILL, J. U., MENZEL, M. T., and BARNES, D. C., Third Topical Conference on Pulsed High-Beta Plasma, Culham, England (Pergamon, New York, 1976), p. 375.

[9] GRIBBLE, R. F., QUINN, W. E., and SIEMON, R. E., Phys. Fluids 14 9 (1971) 2042.

[10] THOMAS, K. S., HARRIS, H. W., JAHODA, F. C., SAWYER, G. A., and SIEMON, R. E., Phys. Fluids 17 6 (1975) 1314.

[11] COMMISSO, R. J., EKDAHL, C. A., FREESE, K. B., McKENNA, K. F., and QUINN, W. E., Phys. Rev. Lett. 39 3 (1977) 137.

[12] McKENTY, P., MORSE, R. L., and SOWERS, G. W., (to be published).

[13] WESSON, J. A., in Plasma Physics and Controlled Nuclear Fusion Research, (Proc. 2nd Int. Conf. Culham, 1965) 1 IAEA, Vienna (1966) 223.

[14] WEITZNER, H., Phys. Fluids 20 3 (1977) 384.

[15] MIKHAILOVSKAYA, L. V. and MIKHAILOVSKII, A.-B., Sov. Phys. JETP 18 (1964) 1077.

[16] GROSSMANN, W., KAUFMANN, M. and NEUHAUSER, J., Nucl. Fusion 13 3 (1973) 462.
[17] FREIDBERG, J. P., Phys. Fluids 15 6 (1972) 1102.
[18] TURNER, L., (submitted to the Physics of Fluids), also available as Los Alamos Scientific Laboratory report LA-UR-78-1782.
[19] TURNER, L., Phys Fluids 20 4 (1977) 654 and Phys. Fluids 20 4 (1977) 662.
[20] LEWIS, H. R. and TURNER, L., Nucl. Fusion 16 6 (1976) 993.
[21] LEWIS, H. R., Proceedings of the Annual Controlled Fusion Theory Conference (May 4-6, 1977, San Diego, California), paper H8.
[22] JACOBSON, A. R., BUCHENAUER, C. J., DOWNING, J. N., and THOMAS, K. S., Phys. Rev. Lett. 37 14 (1976) 897.
[23] HOFFMAN, A. L., CRAWFORD, E. A., and LOWENTHAL, D. D., Appl. Phys. Lett. 33 4 (1978) 282.
[24] HOIDA, Hiroshi, Ph.D. Thesis, University of Washington (1978).

FIGURE CAPTIONS

Fig. 1. Stereoscopic streak photograph taken at the coil midplane.

Fig. 2. Time history of the electron and total plasma temperature at the coil midplane, and results from MHD code. Data points from: (●) Thomson scattering, (⊙) pressure balance, (▲) neutron emission rate plus Thomson scattering.

Fig. 3. Time history of the energy line density measured at the coil midplane, and MHD code results for open-ended and end-plugged (no axial flow) theta-pinch configurations.

Fig. 4. Time history of interferometrically determined total plasma inventory.

Fig. 5. Theoretical and experimental results for n versus β_a.

Fig. 6. Ablated and ionized end-plug material radial density profiles for, (a) BN and, (b) LiD end plugs.

Fig. 7. Time history of the energy line density measured at the coil midplane for the open-ended and LiD end-plugged theta-pinch configuration. τ_E is obtained from a least squares fit to the data for $t \geq 6.0$ μs.

Fig. 8. Comparison of the variation of η with M as computed from the two-dimensional, time dependent equations with guiding center theory and data from linear Scyllac.

Fig. 9. Radial streak photograph of laser heated 1.5 mTorr D_2 theta-pinch plasma.

Fig. 10. Laser heated 1.5 mTorr D_2 theta pinch plasma: (a) comparison of experimental and calculated diamagnetic signals, (b) calculated plasma profiles.

Fig. 11. Interferometrically measured radial density profiles for various times in the 22 cm solenoid. Solid curves and dashed curves for unheated and laser heated columns, respectively.

Fig. 12. (a) Interferogram of laser heated plasma in 22 cm solenoid. p_0 = 1.8 mTorr, laser energy 360 J initiated at 220 ns. Picture at 640 ns. (b) Line energy densities versus time for 22 cm laser heated solenoid, measure with diamagnetic loops.

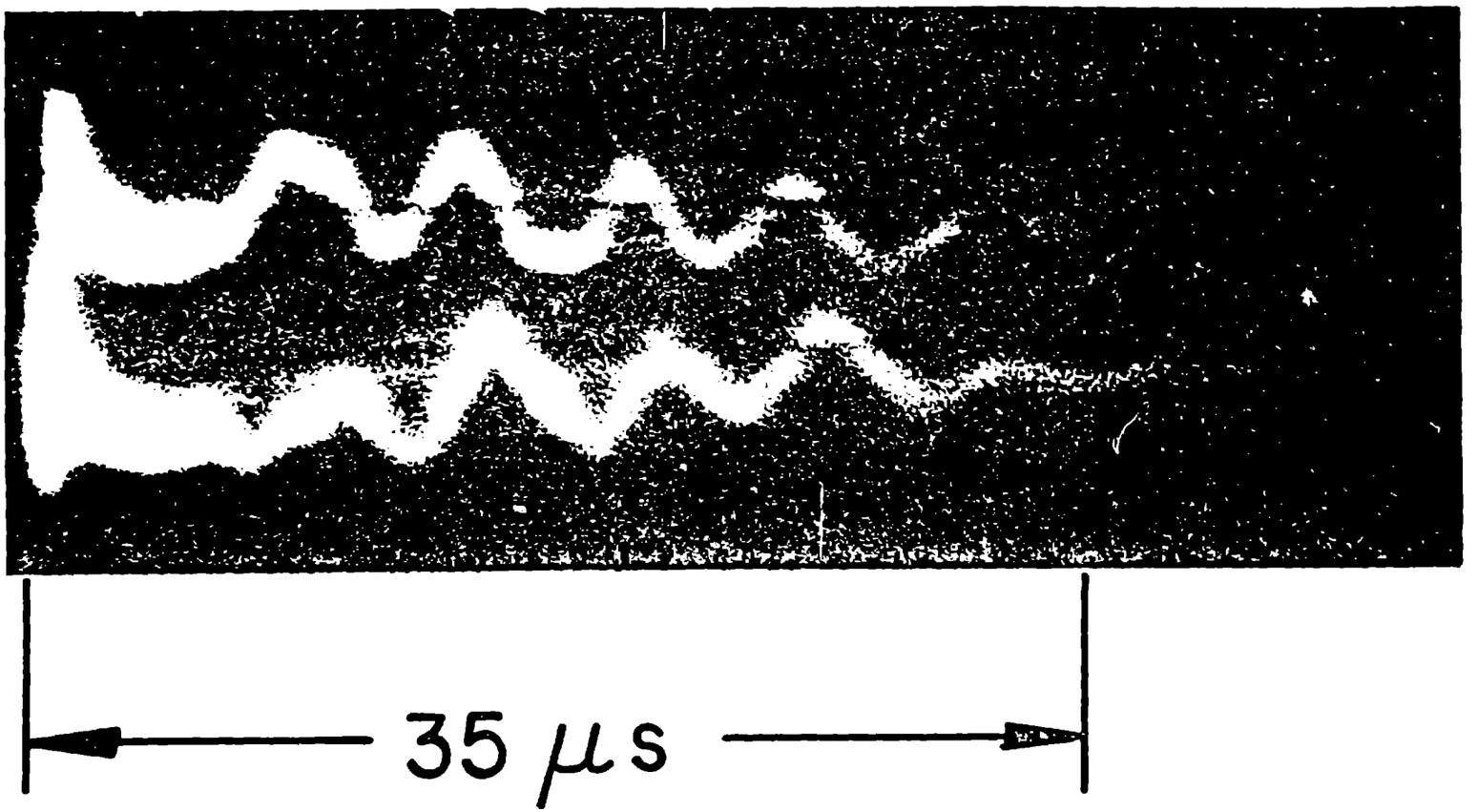

Fig. 1. Stereoscopic streak photograph taken at the coil midplane.

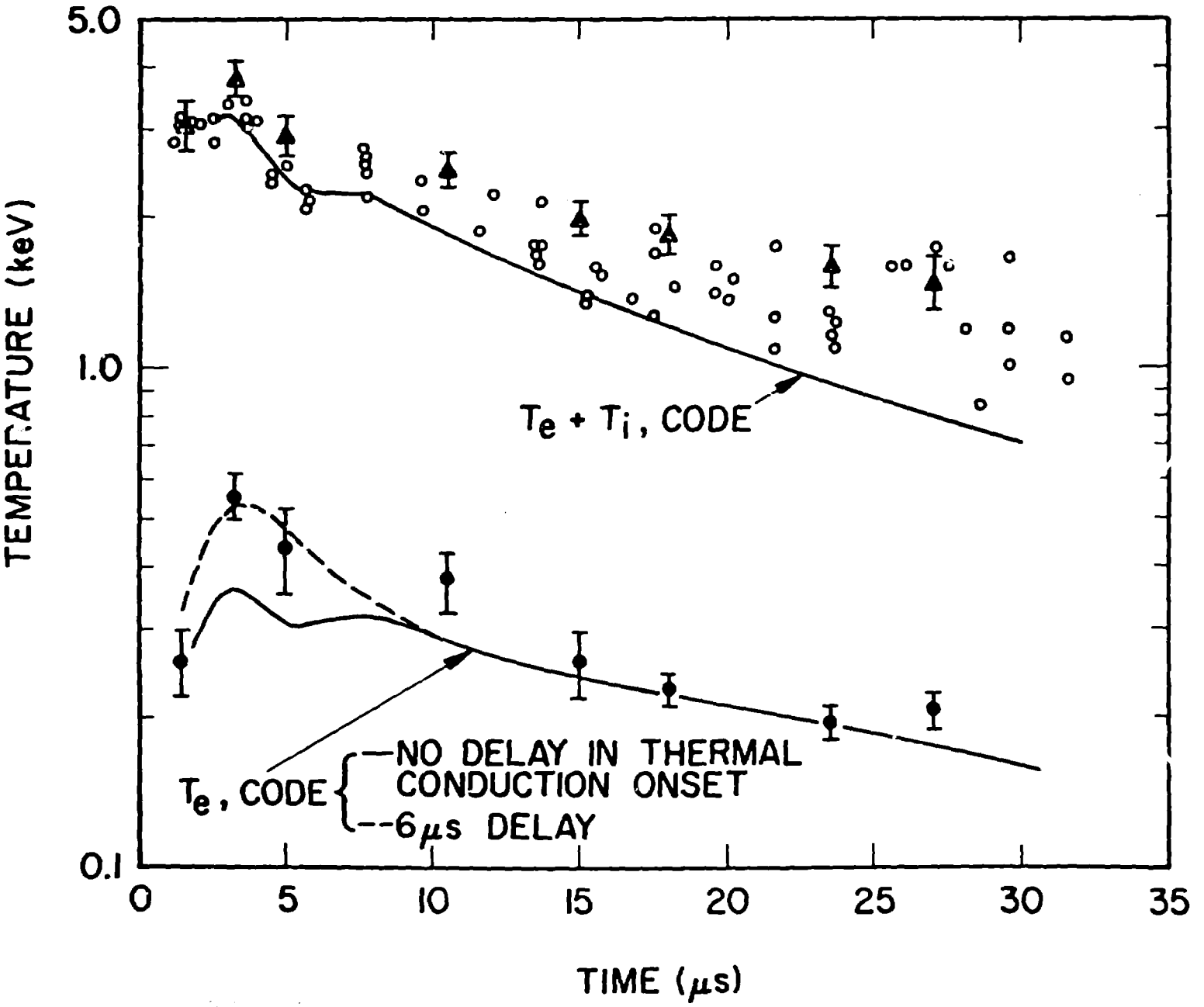

Fig. 2. Time history of the electron and total plasma temperature at the coil midplane, and results from MHD code. Data points from: (●) Thomson scattering, (O) pressure balance, (▲) neutron emission rate plus Thomson scattering.

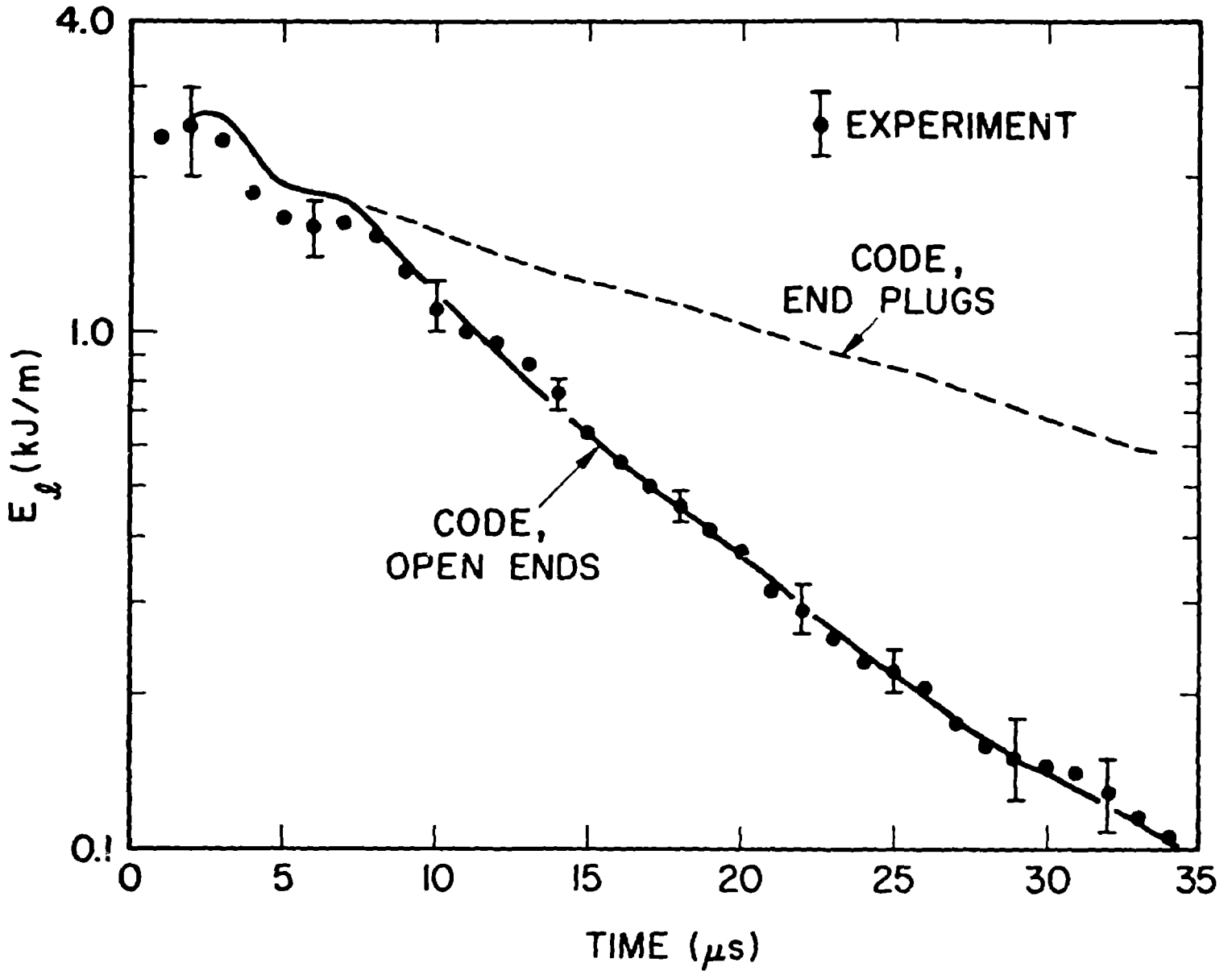

Fig. 3. Time history of the energy line density measured at the coil midplane, and MHD code results for open-ended and end-plugged (no axial flow) theta-pinch configurations.

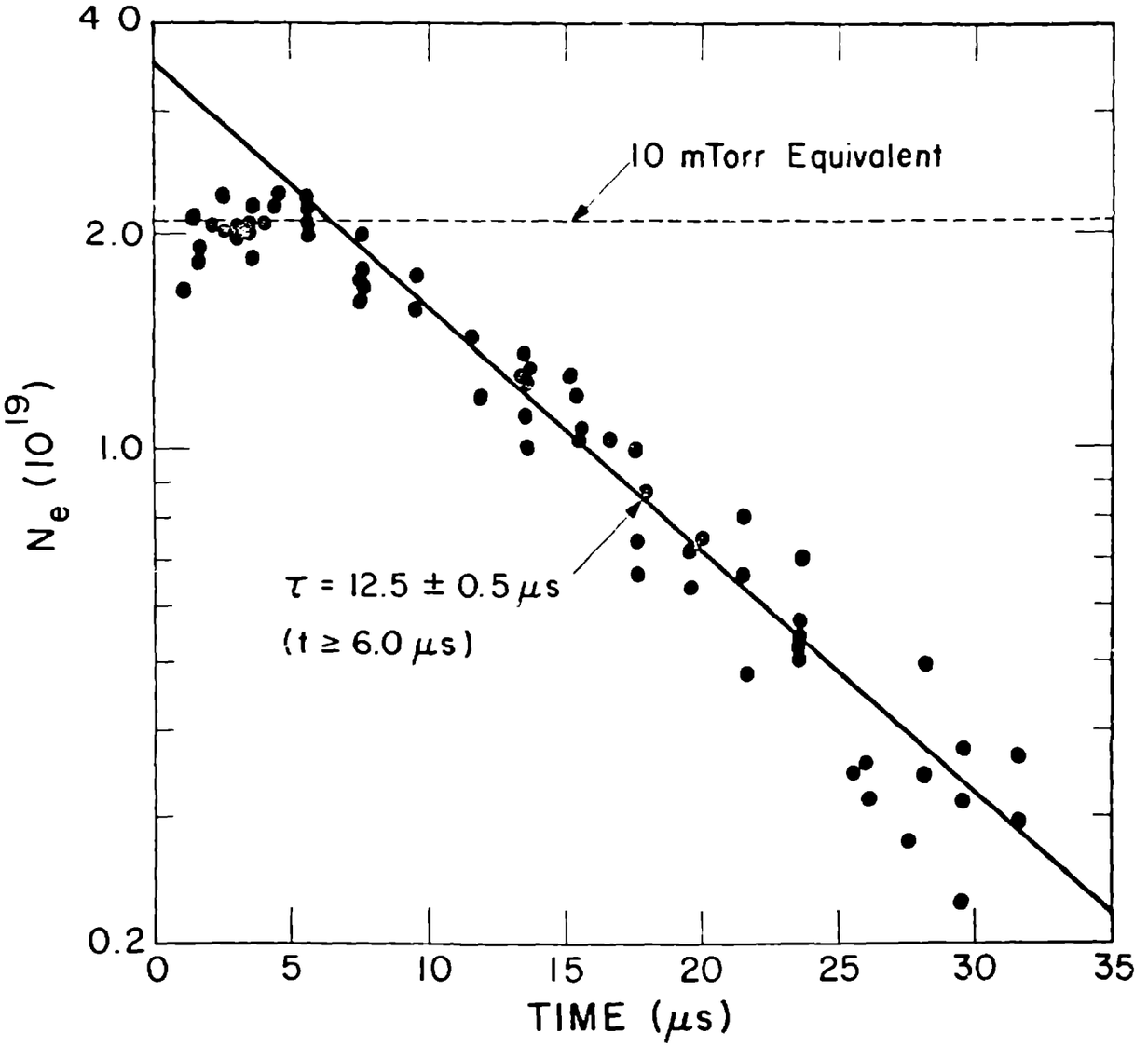

Fig. 4. Time history of interferometrically determined total plasma inventory.

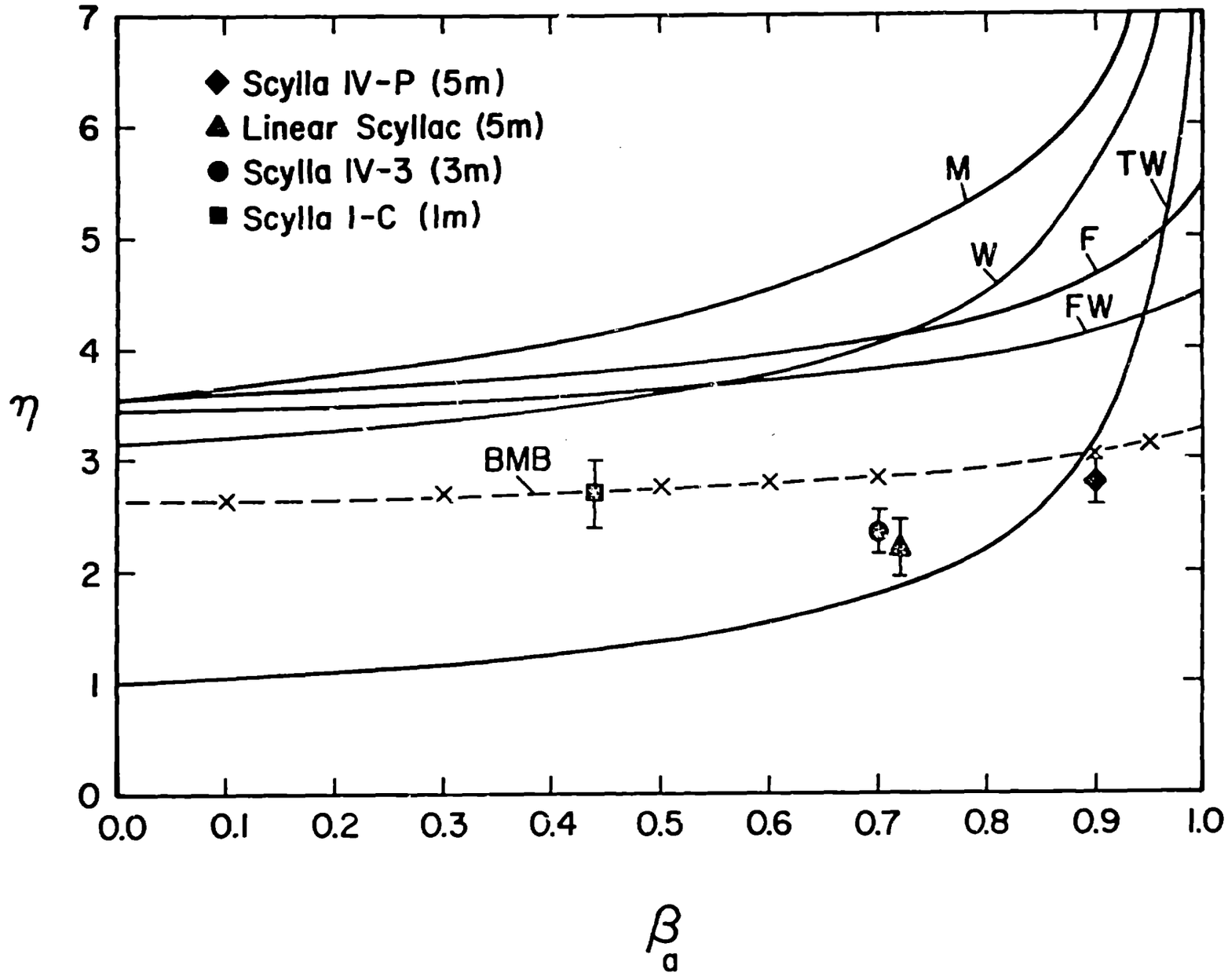

Fig. 5. Theoretical and experimental results for η versus β_a.

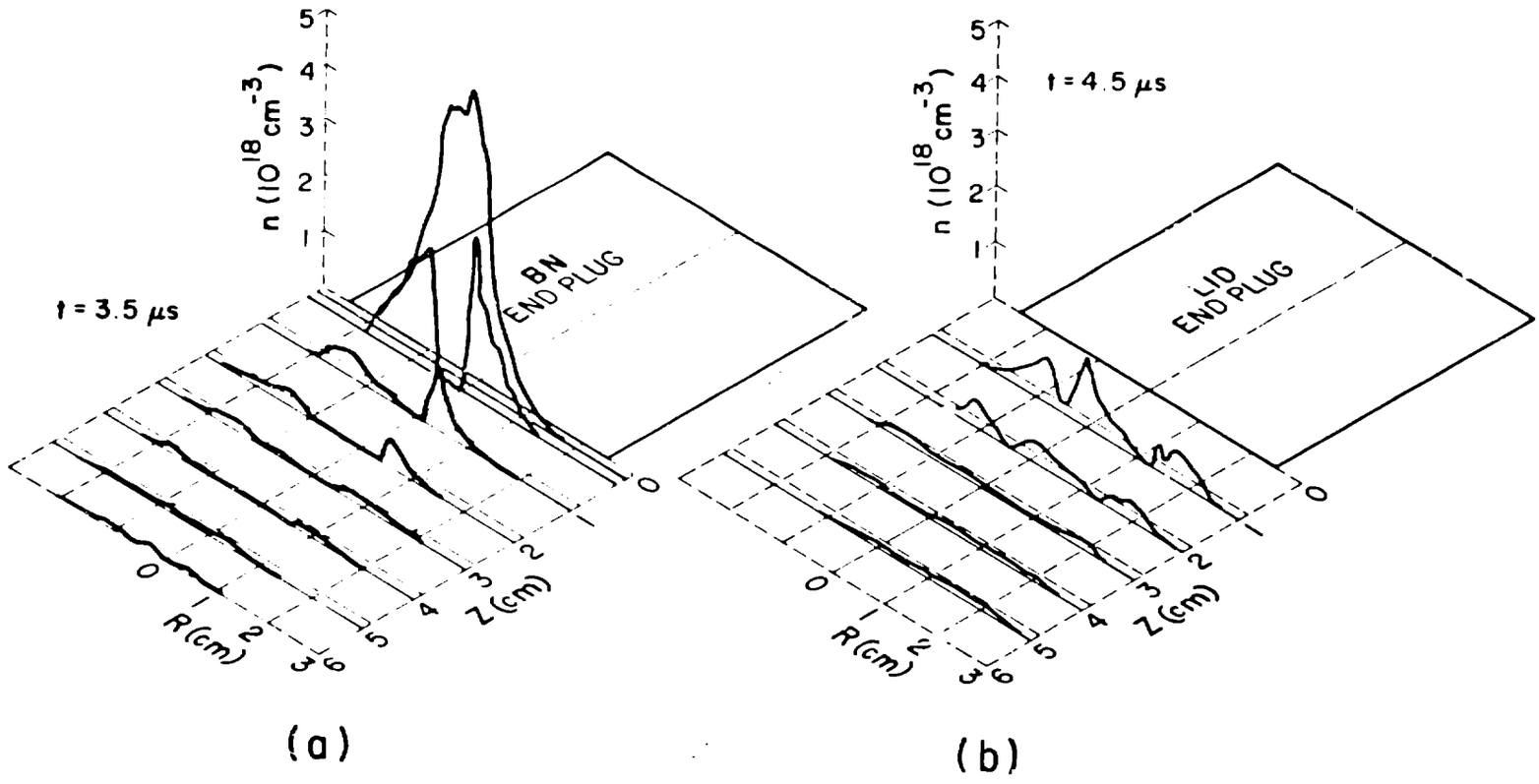

Fig. 6. Ablated and ionized end-plug material radial density profiles for, (a) BN and, (b) LiD end plugs.

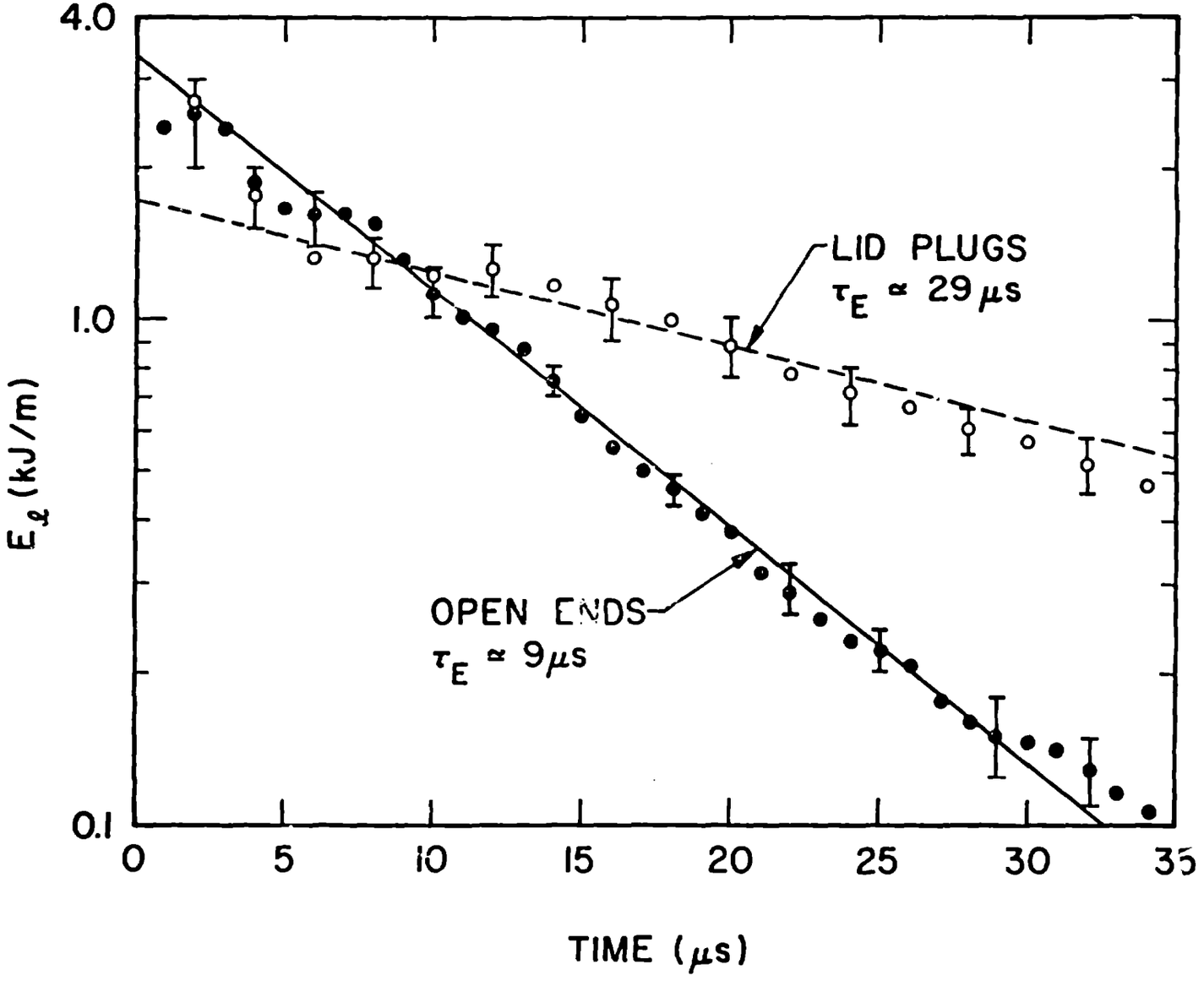

Fig. 7. Time history of the energy line density measured at the coil midplane for the open-ended and LiD end-plugged theta-pinch configuration. τ_E is obtained from a least squares fit to the data for $t \geq 6.0$ μs.

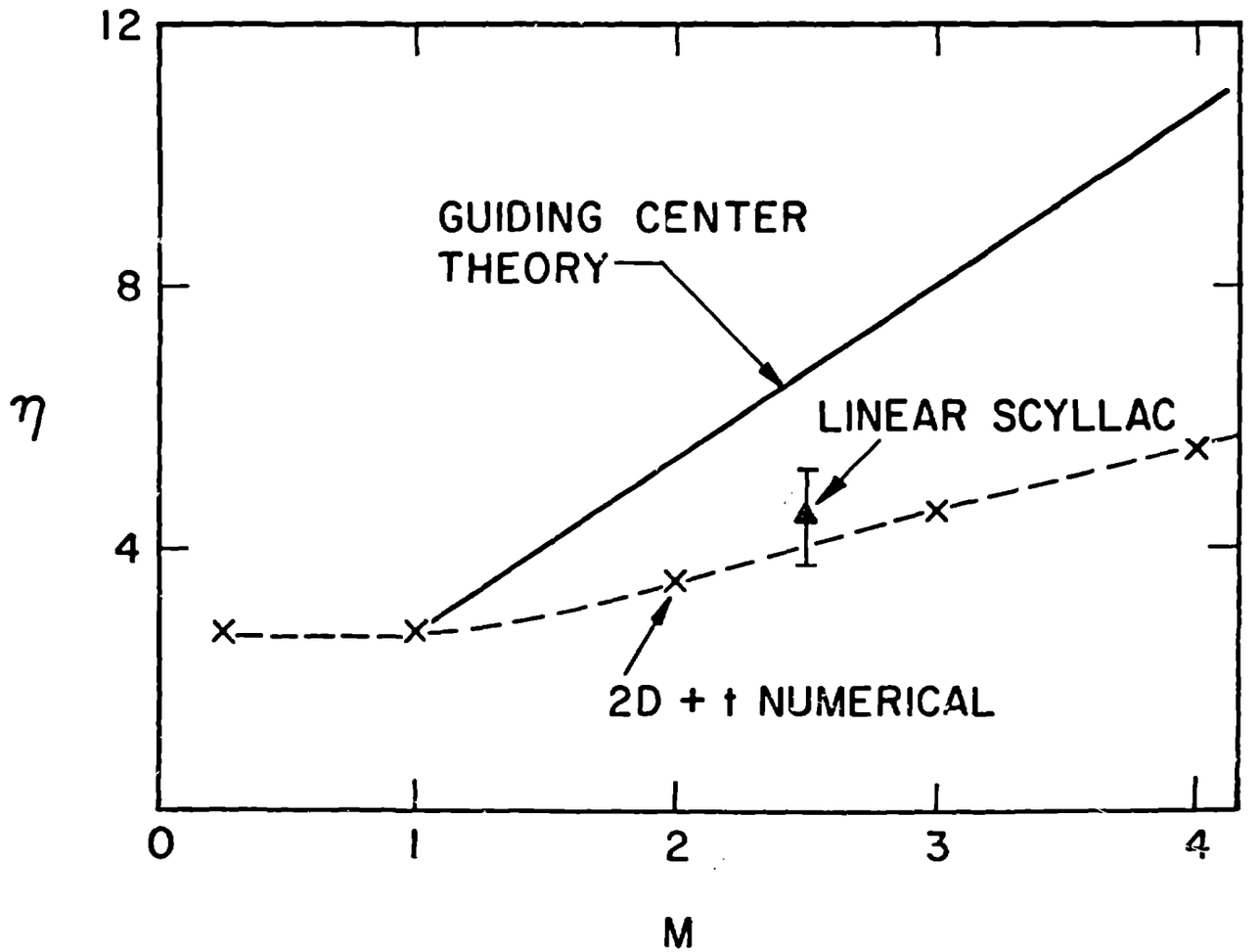

Fig. 8. Comparison of the variation of η with M as computed from the two-dimensional, time dependent equations with guiding center theory and data from linear Scyllac.

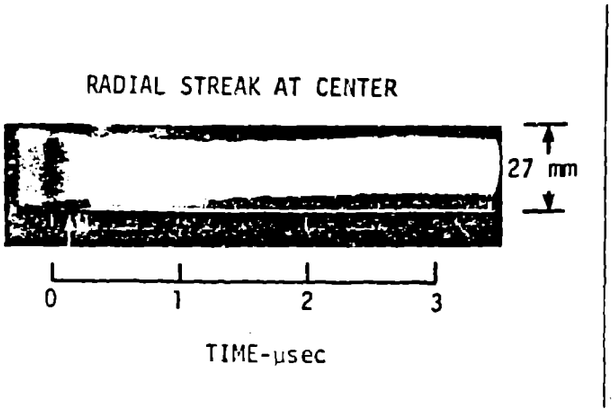

Fig. 9. Radial streak photograph of laser heated 1.5 mTorr D_2 theta-pinch plasma.

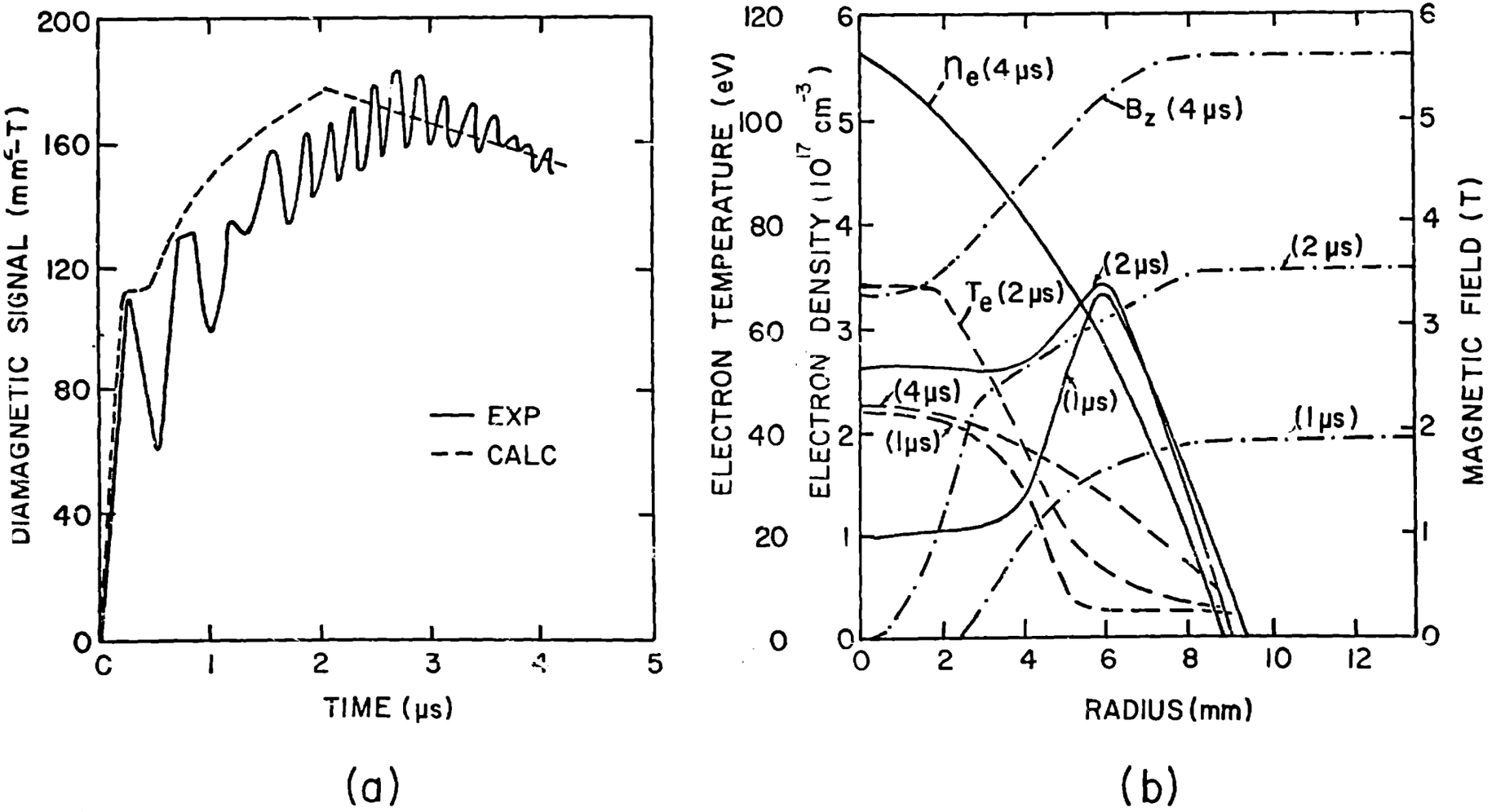

Fig. 10. Laser heated 1.5 mTorr D_2 theta pinch plasma: (a) comparison of experimental and calculated diamagnetic signals, (b) calculated plasma profiles.

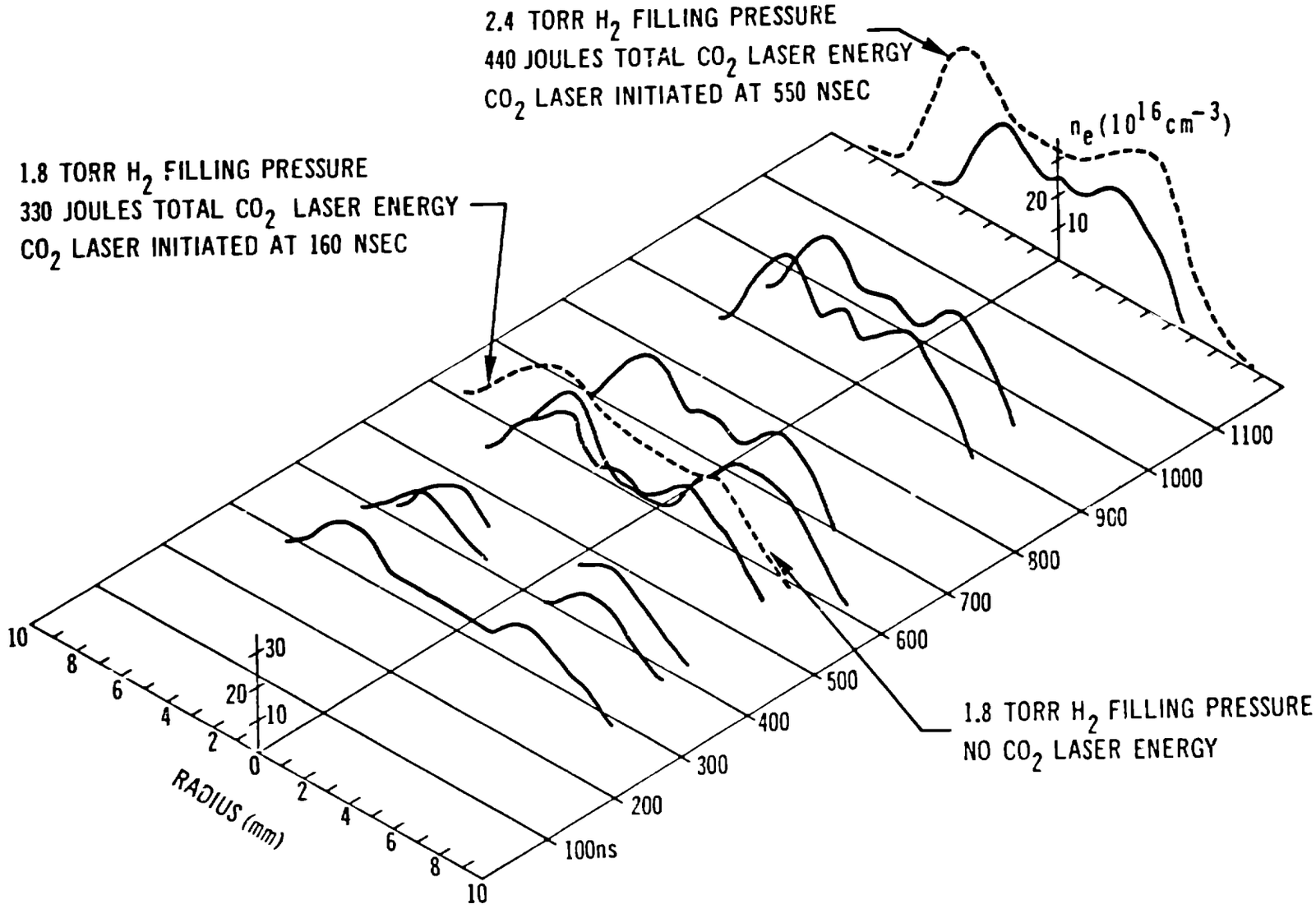

Fig. 11. Interferometrically measured radial density profiles for various times in the 22 cm solenoid. Solid curves and dashed curves for unheated and laser heated columns, respectively.

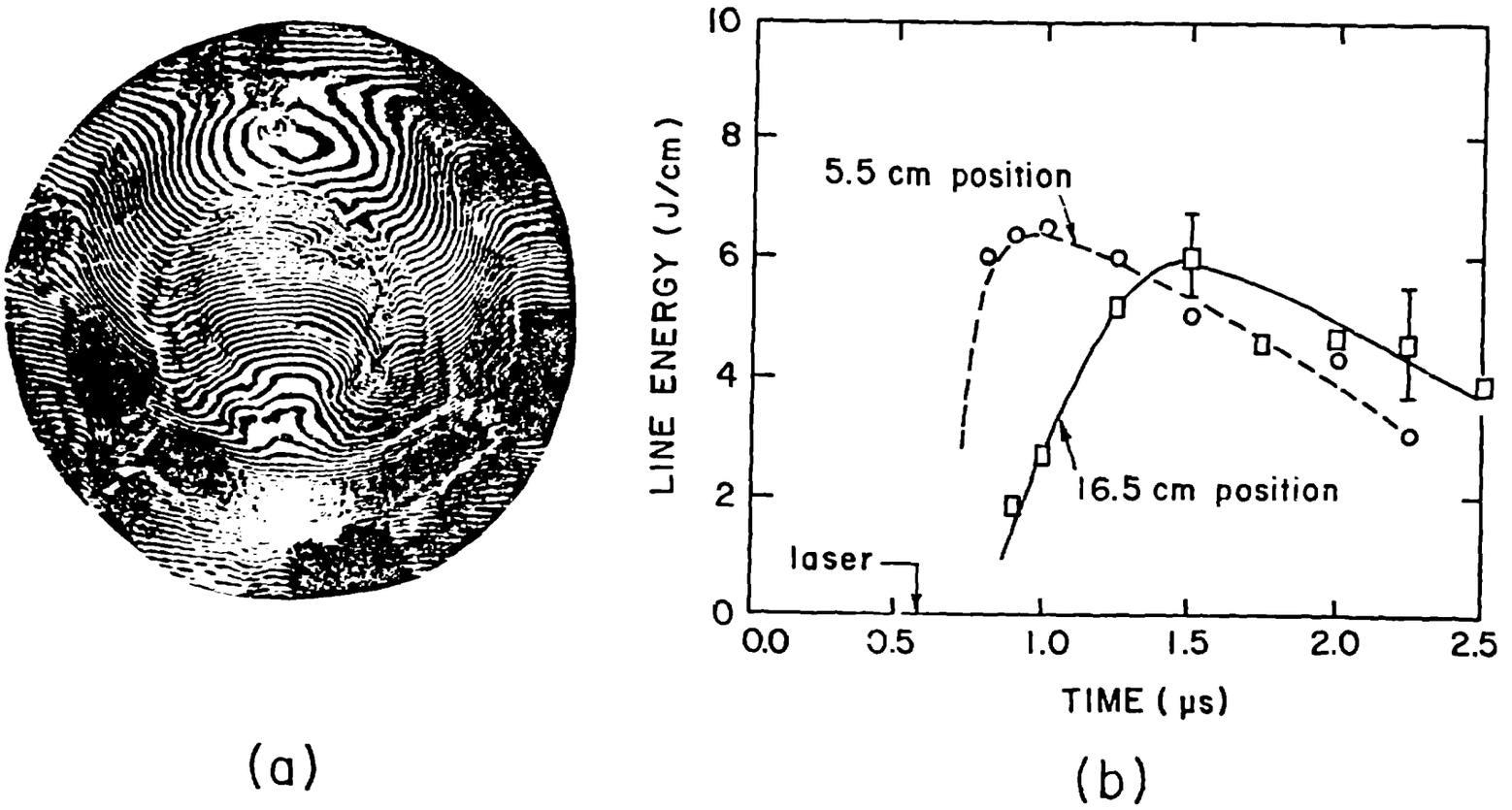

Fig. 12. (a) Interferogram of laser heated plasma in 22 cm solenoid. p_0 = 1.8 mTorr, laser energy 360 J initiated at 220 ns. Picture at 640 ns. (b) Line energy densities versus time for 22 cm laser heated solenoid, measure with diamagnetic loops.